Influence of Magnetic Ordering between Cr Adatoms on the Yu-Shiba-Rusinov States of the β-Bi$_2$Pd Superconductor

Deung-Jang Choi,[1,2,3,4,*] Carlos García Fernández,[2] Edwin Herrera,[5] Carmen Rubio-Verdú,[3] Miguel M. Ugeda,[1,4] Isabel Guillamón,[5] Hermann Suderow,[5] José Ignacio Pascual,[3,4] and Nicolás Lorente[1,2]

[1]*Centro de Física de Materiales CFM/MPC (CSIC-UPV/EHU), 20018 Donostia-San Sebastián, Spain*
[2]*Donostia International Physics Center (DIPC), 20018 Donostia-San Sebastián, Spain*
[3]*CIC nanoGUNE, 20018 Donostia-San Sebastián, Spain*
[4]*Ikerbasque, Basque Foundation for Science, 48013 Bilbao, Spain*
[5]*Laboratorio de Bajas Temperaturas, Departamento de Física de la Materia Condensada, Instituto Nicolás Cabrera and Condensed Matter Physics Center (IFIMAC), Universidad Autónoma de Madrid, E-28049 Madrid, Spain*

We show that the magnetic ordering of coupled atomic dimers on a superconductor is revealed by their intragap spectral features. Chromium atoms on the superconductor β-Bi$_2$Pd surface display Yu-Shiba-Rusinov bound states, detected as pairs of intragap excitations in tunneling spectra. By means of atomic manipulation with a scanning tunneling microscope's tip, we form Cr dimers with different arrangements and find that their intragap features appear either shifted or split with respect to single atoms. These spectral variations are associated with the magnetic coupling, ferromagnetic or antiferromagnetic, of the dimer, as confirmed by density functional theory simulations. The striking qualitative differences between the observed tunneling spectra prove that intragap Shiba states are extremely sensitive to the magnetic ordering on the atomic scale.

Magnetic impurities have a detrimental effect on superconductivity [1]. The exchange interaction between the atomic magnetic moments and Cooper pairs produces localized bound states inside the superconducting (SC) gap, known as Yu-Shiba-Rusinov [2–4] states (Shiba states in the following). Previous scanning tunneling spectroscopy measurements found that Shiba states can be detected in magnetic adatoms on a superconducting surface [5] as very sharp intragap peaks in their quasiparticle excitation spectra [6,7]. The position of the peaks inside the gap is very sensitive to the exchange interaction of the impurity with the surface [8], whereas their number can be related to the amount of spin-polarized atomic orbitals [9,10] and the spin's multiplet in the presence of anisotropy [11].

In spite of the local character of the atomic scattering potential, the amplitude of Shiba wave functions can extend over several nanometers [9,12] and interfere with other Shiba states of close-by impurities [6,13]. It has been predicted that the subgap spectral features of a pair of interacting impurities depend on the alignment of their magnetic moments [14]. Hybridization of Shiba states in atomic-scale structures is a prerequisite for the formation of extended Shiba bands [15], which under certain circumstances may develop exotic properties such as topological superconductivity [16,17]. Therefore, examining the character of Shiba hybridization at the atomic scale and its relation with the magnetic alignment of the impurities is crucial.

Here we study quasiparticle excitation spectra over Cr atomic dimers on the surface of the superconductor β-Bi$_2$Pd and show that they reveal the alignment of their magnetic moments. We use the tip of a scanning tunneling microscope (STM) to manipulate individual Cr atoms and form atomically precise dimers with different interatomic orientations and distances. Differential conductance (dI/dV) measurements on the Cr dimers reveal that their Shiba states shift or split with respect to those on isolated atoms depending on the dimer's arrangement on the surface. Furthermore, the spatial distributions of the hybridized Shiba states resemble either antibonding or bonding components of a "Shiba molecule" [14,18–20]. With the support of density functional theory (DFT) simulations, we conclude that the evolution of Shiba states in each case is originated by either the antiparallel or parallel alignment of the dimer's atomic magnetic moments.

Our experiments were carried out on the Bi-terminated surface of a β-Bi$_2$Pd crystal (see Methods in Supplemental Material [21–26]), cleaved under ultrahigh-vacuum (UHV) conditions, and subsequently transferred *in situ* into a cryogenic STM for measurements at $T = 1.2$ K. The exposed surface is atomically clean and shows a squared atomic structure [Fig. 1(a)], with periodicity in agreement with the β-Bi$_2$Pd unit cell (lattice parameter $a = 3.36$ Å). Next, we evaporated small amounts of Cr atoms on the pristine surface at a low temperature ($T = 15$ K) to obtain Cr densities similar to that shown in the STM image in
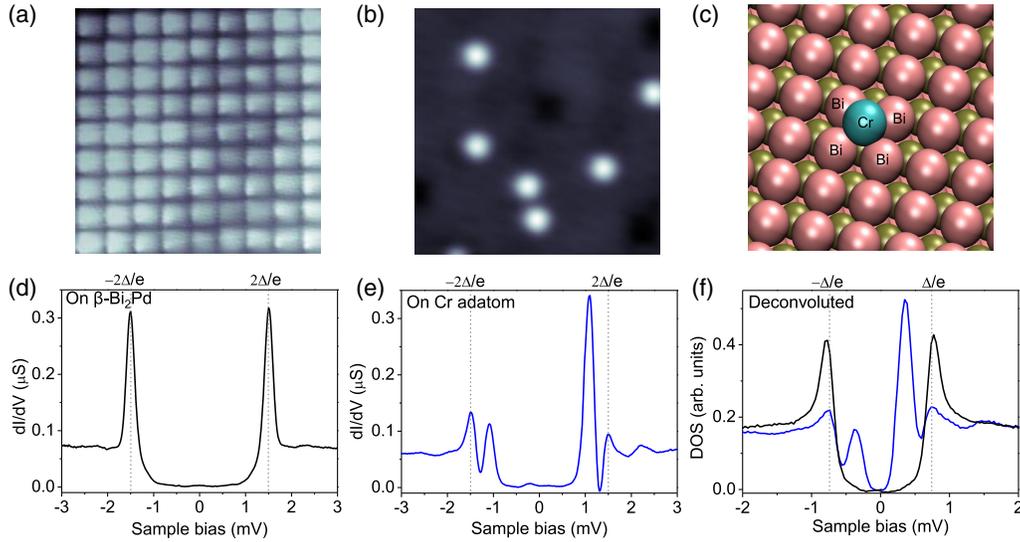
FIG. 1. Cr atoms on the Bi-terminated β-Bi$_2$Pd surface. (a) Atomic resolution of a Bi-terminated clean β-Bi$_2$Pd surface in a constant height mode at 3 mV, 200 nA with the junction resistance of 15 kΩ (size 3×3 nm^2). (b) STM image of Cr atoms deposited on the Bi-terminated β-Bi$_2$Pd surface ($V = 1$ V, $I = 10$ pA, size 10×10 nm^2). (c) Results of a full DFT relaxation showing that the most stable position of a Cr atom (green) is at a hollow site (Bi atoms in pink and Pd atoms in bronze). Differential-conductance spectra measured (d) on the bare surface and (e) on a Cr adatom, using a superconducting β-Bi$_2$Pd tip (feedback loop opening condition 3 mV, 250 pA). Tunneling between coherent peaks of the tip and sample results in sharp dI/dV peaks at $\pm 2\Delta/e$ (dashed lines in the plots). (f) Density of states obtained by deconvoluting the tip DOS from the spectra on the Cr adatom (blue line) and on the bare surface (black line). Analysis of STM and scanning tunneling spectroscopy data was performed with the `WSxM` [27] and `SpectraFox` [28] software packages.

Fig. 1(b). Individual Cr adatoms appear as protrusions 110 pm high. They are absorbed on hollow sites of the bismuth surface (see Supplemental Material [21]). This agrees with the minimum energy configuration obtained from DFT simulations, shown in Fig. 1(c) and in Supplemental Material [21].

The stoichiometric compound β-Bi$_2$Pd is an s-wave superconductor with a single gap of magnitude $\Delta = 0.76$ meV [29]. The superconducting properties are very isotropic [30], leading to a narrow gap distribution of just a few tens of μeV wide [29], in spite of its square Fermi surface [31,32]. We determined the LDOS of pristine and Cr-decorated regions by means of differential conductance (dI/dV) spectra. To enhance the spectral resolution, we employed superconducting STM tips obtained by indenting a W tip into the β-Bi$_2$Pd surface, which has an isotropic single superconducting gap. As a consequence, the tunneling spectra result from the convolution of the tip and sample LDOS [6,8]. The dI/dV spectrum of the pristine β-Bi$_2$Pd surface [Fig. 1(d)] shows a conductance gap with two sharp peaks at ± 1.52 mV, i.e., at $\pm 2\Delta/e$, due to tunneling between quasiparticle (QP) peaks at $\pm \Delta$ in the tip and sample. Typical dI/dV spectra acquired on top of single Cr adatoms [Fig. 1(e)] show smaller QP peaks and a pair of additional peaks inside the spectral gap (at $V = \pm 1.1 \pm 0.1$ mV), indicating the formation of Shiba states at the locations of the adsorbed Cr atoms. The absence of Shiba multiplets is probably due to a weaker interaction with the surface as compared with Cr on Pb (111) [6,10], which

keeps Cr orbitals largely degenerate. Figure 1(f) compares the LDOS of a pristine surface and Cr adatoms extracted from the tunneling spectra following the deconvolution procedure of Refs. [10,33].

To explore the effect of magnetic ordering on Cr Shiba states, we studied the evolution of intragap spectral features of Cr atomic dimers constructed by STM lateral manipulation. Before the atomic manipulation, the atomic lattice around the Cr atom is determined from high-resolution images like in Fig. 1(a).

Figures 2(a)–2(d) show STM images of the four types of dimers that show sizable spectral variations. The atoms are separated by (a) $d = \sqrt{5}a$, (b) $d = 2a$, (c) $d = 1a$, and (d) $d = \sqrt{2}a$, corresponding to distances between hollow sites. For larger Cr-Cr separations, the dI/dV spectra are unaffected by the neighboring adatom. In every case, we measured the dI/dV spectrum of a target Cr adatom first isolated [gray lines in Figs. 2(e)–2(h)] and then after a second adatom is precisely positioned nearby [red lines in Figs. 2(e)–2(h)]. The spectrum on the $d = \sqrt{5}a$ dimer shows only a faint effect of the interaction between atoms [Fig. 2(e)]. When their separation is reduced to $d = 2a$, the Shiba peaks appear closer to the SC gap edge [at $V = \pm 1.2 \pm 0.1$ mV, Fig. 2(f)], overlapping with the QP peaks of the superconductor and evolving into broader spectral features. Finally, at very short distances ($d = 1a$), the Shiba excitations are absent from the spectrum, which now show symmetric but broader QP peaks [Fig. 2(g)]. The observed tendency is that
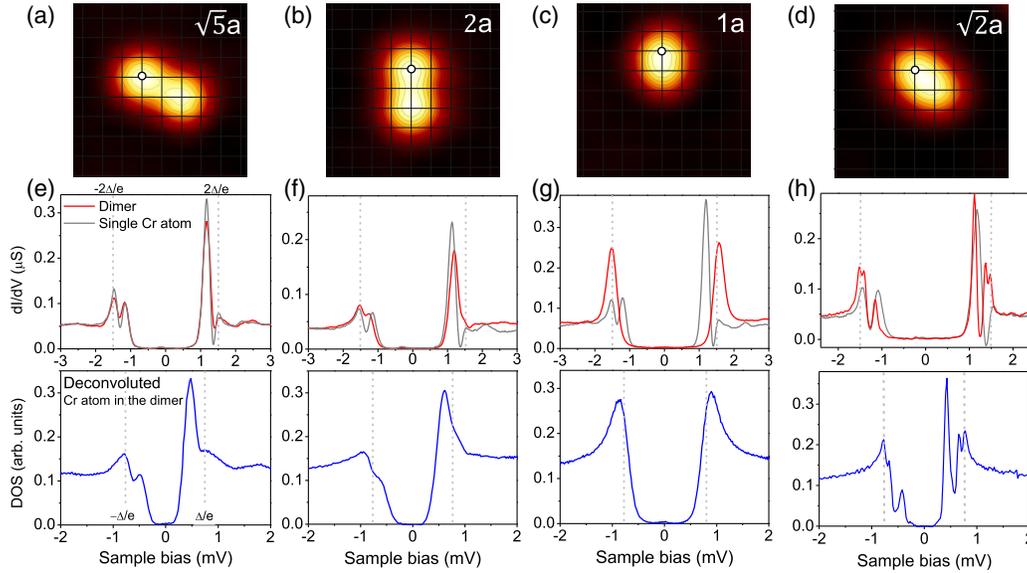
FIG. 2. (a)–(d) STM image of Cr dimers at indicated spacings ($V = 1$ V and $I = 10$ pA, size 3×3 nm^2). The crossing of square mesh depicts the hollow sites of the β-Bi$_2$Pd surface. (e)–(h) Differential conductance spectra on the Cr atom indicated by a white dot before (gray lines) and after (red lines) the second atom is moved to the dimer position (feedback loop opening condition 3 mV, 250 pA). As in Fig. 1, all spectra are measured using superconducting tips with the same Δ as the substrate (dashed lines mark the $\pm 2\Delta/e$ bias in the middle panels and the $\pm \Delta/e$ bias in the bottom panels). The corresponding tip-deconvoluted DOS of the corresponding Cr/β-Bi$_2$Pd system is shown in the lower panels.

Shiba peaks shift towards the QP continuum as the interatomic distance decreases (see more details in Ref. [21]).

Interestingly, when the Cr adatoms are moved to contiguous hollow sites along the surface diagonal, $d = \sqrt{2}a$, the spectra show a more complex structure with additional features close to the QP peaks [Fig. 2(h)]. In this case, the DOS is composed of two intragap peaks for particle states and two peaks for hole states with a separation of $\sim 250 \pm 50$ μeV. This pattern resembles the splitting of hybridized Shiba states predicted for atoms interacting ferromagnetically [14,18–20].

To interpret the observed evolution of intragap spectra in terms of the magnetic alignment of the Cr spins, we show in Fig. 3 the simulated DOS of an antiferromagnetic (AFM) or ferromagnetic (FM) dimer at $d = 2a$ and $d = \sqrt{2}a$ and the corresponding dI/dV spectrum, obtained using an extension of the Flatté and Reynolds model [14] (details in Supplemental Material [21]). The model parametrizes first the electron-Cr interaction of a Cr monomer on the β-Bi$_2$Pd substrate to fit their experimental spectral features. Using this parametrization, the model produces the Shiba DOS for AFM and FM coupled dimers separated by $\sqrt{2}a$ and $2a$ apart (Fig. 3). By comparing the simulated dI/dV curves with the experimental ones, we conclude that the splitting of Shiba states for the $\sqrt{2}a$ dimer stems from their FM coupling, while the single pair of Shiba peaks of the $2a$ dimer reflects AFM interactions.

The model further captures the additional role of potential scattering in the subgap states, which induces a small asymmetry in the particle and hole energy of the states for both AFM and FM cases. These results thus confirm that interacting Shiba states of Cr atoms can evolve into molecularlike states with bonding and antibonding configurations depending on the type of magnetic order.

The different type of Shiba hybridization is reflected in their respective spatial distribution of bound-state excitation amplitude [14]. Figures 4(a) and 4(c) show the spectral maps (i.e., dI/dV vs distance and bias) measured along the axis of the $2a$ and $\sqrt{2}a$ dimers, respectively. In all cases, the amplitude of the QP peaks decreases substantially over the dimer, and a distinct pattern of subgap excitations emerges for every atomic arrangement. For the $2a$ dimer, the amplitude of the Shiba peaks is clearly maximum over each atom and shows a nodal plane in between, for both particle and hole components [Fig. 4(b)]. This is in good agreement with predictions for the AFM case [14], picturing the hybridized Shiba states as degenerate states localized around each of the two impurities. In contrast, the $\sqrt{2}a$ dimer shows a different pattern for each of the split Shiba states. The state with lower energy appears with more amplitude in the region between the two atoms, while the higher one shows a nodal plane between them [see Fig. 4(c)]. This is clearly visualized in dI/dV spatial maps at each excitation energy [Fig. 4(d)], showing a bonding and antibonding pattern for the lower and higher Shiba states, respectively.

The DFT further confirms the magnetic ordering of the adsorbed dimers. A single Cr adatom preferentially adsorbs
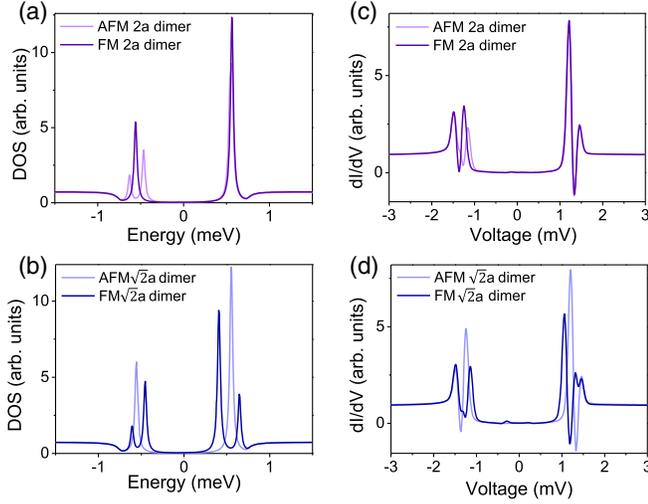
FIG. 3. Model calculation of the Shiba DOS of an antiferro-magnetically or ferromagnetically ordered dimer separated by (a) $d = 2a$ and (b) $d = \sqrt{2}a$ (see details [21]). For both dimer structures, FM order leads to split Shiba peaks, while AFM shows only a degenerate one. Panels (c) and (d) show the corresponding dI/dV spectra obtained by convoluting the dimer's DOS with a superconducting tip DOS.

on the hollow site, with a subsurface Pd atom directly underneath [Fig. 1(c)]. The adatom's next-neighbor Pd and Bi atoms slightly approach towards the Cr adatom by 10 and 5 pm, respectively, inducing a small distortion of the surface (see Supplemental Material). The Cr adatom lies 1.59 Å above the surface layer and keeps a total magnetic moment of $4.4\mu_B$, close to the $5\mu_B$ of a free atom. The large spin polarization of the system can be pictured by isosurfaces of the electronic density difference between majority and minority spins, shown in Fig. 5(a). The Cr atom polarizes the four nearest-neighbor Bi atoms antiferromagnetically and the second-layer Pd atoms ferromagnetically.

According to DFT, the most stable dimer configuration on the surface has both atoms absorbed on contiguous hollow sites separated by a distance $d = 1a$. This corresponds to the compact dimer shown in Figs. 2(c) and 5(b). The two atoms interact strongly and approach, reducing the Cr-Cr distance by 72 pm (from $a = 3.46$ Å to $d = 2.74$ Å). They are antiferromagnetically coupled with an energy 152 meV lower than the ferromagnetic configuration ($E_{AFM} - E_{FM} = \Delta E = -152$ meV). The $2a$ dimer shows a much weaker interatomic interaction, and each Cr appears with a negligible deviation from the single adatom adsorption geometry. Their atomic spins interact via the substrate with a slight preference for antiferromagnetic ordering ($\Delta E = -10$ meV), in agreement with the assignment from the experiments. The spin density of the $2a$ configuration [Fig. 5(c)] pictures this antiferromagnetic arrangement. Furthermore, the intermediate Bi atoms have a stronger magnetic polarization and probably mediate the interaction between Cr adatoms.
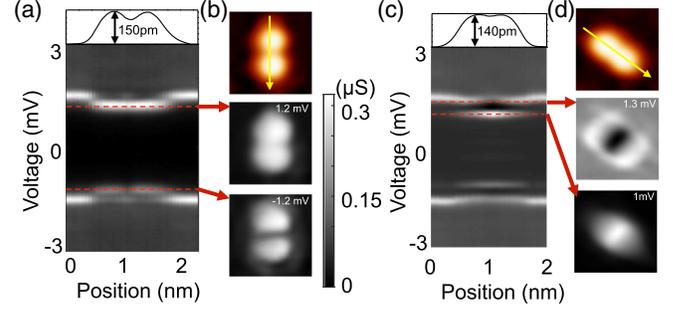

FIG. 4. Topography profiles and spectral (dI/dV vs V) maps measured along the axes of the (a) $2a$ and (c) $\sqrt{2}a$ dimers (gray scale covers the dI/dV range from 0 to 0.3 μS). The top panels in (b) and (d) correspond to the dimer STM image, scanned at 3 meV and 10 pA. Below, we show the 2D spatial distribution of the differential conductance at the bias of the Shiba peaks for (b) the $2a$ dimer (size 3×3 nm^2) and (d) the $\sqrt{2}a$ dimer (size 2.5×2.5 nm^2), at the given energies.

The dimer along neighboring diagonal sites [$d = \sqrt{2}a$ in Figs. 2(d) and 5(d)] shows a preference for a ferro-magnetic ground state, with $\Delta E = 19$ meV, again in good agreement with the interpretation of Shiba spectral features. Interestingly, both Cr atoms appear connected via a single Bi atom [Fig. 5(d)], which shows opposite magnetization and, probably, forces the ferromagnetic ordering of the dimer.

The DFT results thus confirm the magnetic ordering deduced from the analysis of Shiba states. Both $1a$ and $2a$ dimers are antiferromagnetically aligned, in agreement
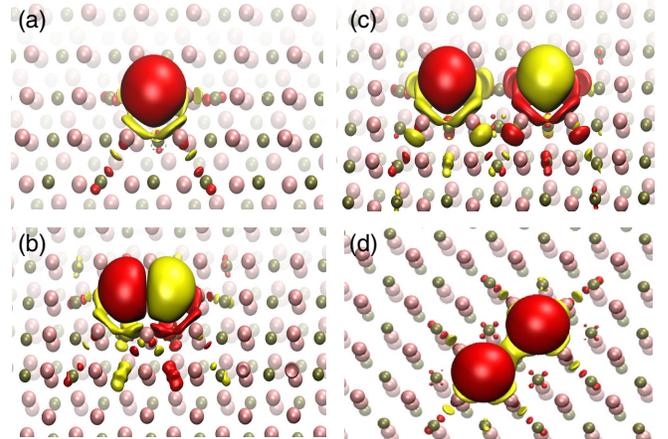

FIG. 5. Spin polarization (a) of a Cr adatom and of various dimers [$d = 1a$ (b), $2a$ (c), and $\sqrt{2}a$ (d)] on the β-Bi$_2$Pd surface. In each case, the results correspond to the minimum-energy configuration obtained from DFT simulations of the relaxed system. The plot shows 3D isosurfaces of constant electronic density difference between majority and minority spins, in the normal state. The surface is tilted differently in every case to picture the extension of the spin density to inner layers. Bi atoms are represented in pink and Pd atoms in bronze. The isocontours of spin are yellow and red for each of the two spin components (the isocontour is $0.005e/$ Å^3 in all graphs).

with the measurement of a single pair of intragap excitations. The observed shift of the Shiba excitations towards the gap edge with a reducing Cr-Cr distance reflects the weakening of the bound state's energy, probably due to the reduction of the total magnetization of antiferromagnetically coupled dimers. For the $\sqrt{2}a$ dimer, the splitting of Shiba states and their peculiar bonding-antibonding spatial distribution reflect the ferromagnetic coupling of the dimer.

In summary, we demonstrated that the spectral features of coupled Shiba states reflect the magnetic ordering of interacting atoms. We proved this by studying dimers of Cr atoms on a superconducting β-Bi$_2$Pd surface, assembled by atomic manipulation using a low-temperature STM. Differential conductance spectra reveal subgap excitations associated with Shiba states, which evolve as the atoms are brought to proximity, reflecting their mutual spin alignment. We found that different atomic arrangements on the surface result in shifts or splits of the atomic Shiba features. Furthermore, the spatial distribution of the Shiba peaks for the $\sqrt{2}a$ dimer resembles bonding and antibonding states, as predicted for a ferromagnetic dimer. DFT simulations confirm the magnetic ordering deduced from the spectra analysis.

Note added in proof.—Recently, we became aware of similar work on wave-function hybridization on YSR pairs on the Pb(111) surface [34].

---

*Corresponding author.
djchoi@dipc.org

[1] B. T. Matthias, H. Suhl, and E. Corenzwit, Phys. Rev. Lett. **1**, 92 (1958).
[2] L. Yu, Acta Phys. Sin. **21**, 75 (1965).
[3] H. Shiba, Prog. Theor. Phys. **40**, 435 (1968).
[4] A. I. Rusinov, Sov. Phys. JETP **29**, 1101 (1969).
[5] A. Yazdani, B. A. Jones, C. P. Lutz, M. F. Crommie, and D. M. Eigler, Science **275**, 1767 (1997).

[6] S.-H. Ji, T. Zhang, Y.-S. Fu, X. Chen, X.-C. Ma, J. Li, W.-H. Duan, J.-F. Jia, and Q.-K. Xue, Phys. Rev. Lett. **100**, 226801 (2008).
[7] M. Ruby, F. Pientka, Y. Peng, F. von Oppen, B. W. Heinrich, and K. J. Franke, Phys. Rev. Lett. **115**, 087001 (2015).
[8] K. J. Franke, G. Schulze, and J. I. Pascual, Science **332**, 940 (2011).
[9] M. Ruby, Y. Peng, F. von Oppen, B. W. Heinrich, and K. J. Franke, Phys. Rev. Lett. **117**, 186801 (2016).
[10] D.-J. Choi, C. Rubio-Verdú, J. de Bruijckere, M. M. Ugeda, N. Lorente, and J. I. Pascual, Nat. Commun. **8**, 15175 (2017).
[11] N. Hatter, B. W. Heinrich, M. Ruby, J. I. Pascual, and K. J. Franke, Nat. Commun. **6**, 8988 (2015).
[12] G. C. Ménard *et al.*, Nat. Phys. **11**, 1013 (2015).
[13] S. Kezilebieke, M. Dvorak, T. Ojanen, and P. Liljeroth, Nano Lett., DOI: 10.1021/acs.nanolett.7b05050 (2018).
[14] M. E. Flatté and D. E. Reynolds, Phys. Rev. B **61**, 14810 (2000).
[15] M. Ruby, F. Pientka, Y. Peng, F. von Oppen, B. W. Heinrich, and K. J. Franke, Phys. Rev. Lett. **115**, 197204 (2015).
[16] Y. Oreg, G. Refael, and F. von Oppen, Phys. Rev. Lett. **105**, 177002 (2010).
[17] S. Nadj-Perge, I. K. Drozdov, J. Li, H. Chen, S. Jeon, J. Seo, A. H. MacDonald, B. A. Bernevig, and A. Yazdani, Science **346**, 602 (2014).
[18] D. K. Morr and J. Yoon, Phys. Rev. B **73**, 224511 (2006).
[19] N. Y. Yao, C. P. Moca, I. Weymann, J. D. Sau, M. D. Lukin, E. A. Demler, and G. Zaránd, Phys. Rev. B **90**, 241108 (2014).
[20] Y. Kim, J. Zhang, E. Rossi, and R. M. Lutchyn, Phys. Rev. Lett. **114**, 236804 (2015).
[21] See Supplemental Material at http://link.aps.org/supplemental/10.1103/PhysRevLett.120.167001 for a description of the model Hamiltonian calculations of the coupled Shiba states and the DFT results, as well as additional experimental data, which includes Refs. [24–28].
[22] M. E. Flatté and J. M. Byers, Phys. Rev. Lett. **78**, 3761 (1997).
[23] E. Vernier, D. Pekker, M. W. Zwierlein, and E. Demler, Phys. Rev. A **83**, 033619 (2011).
[24] G. Kresse and J. Furthmüller, Comput. Mater. Sci. **6**, 15 (1996).
[25] J. P. Perdew, K. Burke, and M. Ernzerhof, Phys. Rev. Lett. **77**, 3865 (1996).
[26] I. R. Shein and A. L. Ivanovskii, J. Supercond. Novel Magn. **26**, 1 (2013).
[27] I. Horcas, R. Fernández, J. M. Gómez-Rodríguez, J. Colchero, J. Gómez-Herrero, and A. M. Baro, Rev. Sci. Instrum. **78**, 013705 (2007).
[28] M. Ruby, SoftwareX **5**, 31 (2016).
[29] E. Herrera *et al.*, Phys. Rev. B **92**, 054507 (2015).
[30] J. Kačmarčík *et al.*, Phys. Rev. B **93**, 144502 (2016).
[31] K. Iwaya, Y. Kohsaka, K. Okawa, T. Machida, M. S. Bahramy, T. Hanaguri, and T. Sasagawa, Nat. Commun. **8**, 976 (2017).
[32] M. Sakano, K. Okawa, M. Kanou, H. Sanjo, T. Okuda, T. Sasagawa, and K. Ishizaka, Nat. Commun. **6**, 8595 (2015).
[33] J.-D. Pillet, C. H. L. Quay, P. Morfin, C. Bena, A. L. Yeyati, and P. Joyez, Nat. Phys. **6**, 965 (2010).
[34] M. Ruby, B. W. Heinrich, Y. Peng, F. von Oppen, and K. J. Franke, Phys. Rev. Lett. **120**, 156803 (2018).